JGR Solid Earth

RESEARCH ARTICLE
10.1029/2024JB030528

Microseism Amplitude and Wave Power in the Mediterranean Sea (1996–2023)

Alfio Marco Borzì[1], Andrea Cannata[1,2], Francesco Panzera[1], Sebastiano D'Amico[3], Carlo Lo Re[4], and Richard C. Aster[5]

[1]Dipartimento di Scienze Biologiche, Geologiche ed Ambientali - Sezione di Scienze della Terra, Università degli Studi di Catania, Catania, Italy, [2]Istituto Nazionale di Geofisica e Vulcanologia - Sezione di Catania, Osservatorio Etneo, Catania, Italy, [3]Department of Geosciences, University of Malta, Msida, Malta, [4]Italian Institute for Environmental Protection and Research (ISPRA), Rome, Italy, [5]Department of Geosciences, Warner College of Natural Resources, Colorado State University, Fort Collins, CO, USA

Key Points:

- 27 year trends of microseism energy and wave power were retrieved for Mediterranean seismic stations and surrounding sea areas
- Correlation analysis between microseism amplitude and sea wave features was performed
- Mediterranean microseism energy trends show distinct areal patterns influenced by local conditions

Supporting Information:

Supporting Information may be found in the online version of this article.

Correspondence to:

A. M. Borzì,
alfio.borzi@phd.unict.it;
marcoborzi23@gmail.com

Citation:

Borzì, A. M., Cannata, A., Panzera, F., D'Amico, S., Lo Re, C., & Aster, R. C. (2025). Microseism amplitude and wave power in the Mediterranean Sea (1996–2023). *Journal of Geophysical Research: Solid Earth*, *130*, e2024JB030528. https://doi.org/10.1029/2024JB030528

Received 12 OCT 2024
Accepted 20 DEC 2024

Author Contributions:

Conceptualization: Alfio Marco Borzì, Andrea Cannata
Formal analysis: Alfio Marco Borzì
Investigation: Carlo Lo Re
Methodology: Alfio Marco Borzì, Francesco Panzera, Sebastiano D'Amico, Richard C. Aster
Supervision: Richard C. Aster
Validation: Andrea Cannata, Francesco Panzera, Sebastiano D'Amico, Carlo Lo Re, Richard C. Aster
Writing – original draft: Alfio Marco Borzì
Writing – review & editing: Alfio Marco Borzì, Andrea Cannata, Francesco Panzera, Sebastiano D'Amico, Carlo Lo Re, Richard C. Aster

Abstract In this work, we integrate seismic data recorded by nine coastal Mediterranean seismic stations and wave hindcast data for 1 January 1996 through 15 October 2023. We examine the relationships between the ocean wave-generated microseism signal (the most continuous and ubiquitous seismic signal on Earth) in terms of temporally varying spectral content, root mean square amplitude, and microseism power spectral density, with the main features of principal ocean wave attributes, specifically significant wave heights, wave period and wave power. To explore relationships between microseism and sea state, we performed a correlation analysis between seismic root square mean amplitude and significant wave height time series for the entire Mediterranean Sea for 1996–2023, including retrieving long-term trends for microseism energy and independently estimated wave power and calculating the Spearman correlation coefficient between the two trend time series. Despite the small number of stations available the analysis allows for a useful exploratory study on the microseism and its relationship with Mediterranean Sea state and wave power spanning 27 years. Given the recent increase in the number of regional seismic stations, the growth of data sharing, and the intensification of global warming and climate extreme events, the results and methods explored here can be further implemented and developed in coming years for coastal monitoring purposes in complement with other data sources.

Plain Language Summary In the current context of climate change, where extreme events are becoming increasingly frequent, it is important to analyze sea wave features. We integrated seismic data recorded by nine coastal Mediterranean seismic stations with sea wave data to investigate how an imperceptible and continuous seismic signal arising from ocean waves, called microseism, relates to key sea wave characteristics, such as wave height and power. We conducted a correlation analysis between microseism amplitudes and significant wave height in the Mediterranean Sea from 1996 to 2023 and retrieved the long-term trends of both parameters. Despite a limited number of seismic stations, the study provided valuable insights into the relationship between microseism and sea conditions in the Mediterranean area over a 27 year period. Considering the increasing number of Mediterranean seismic stations and increase in data sharing, along with the intensification of extreme climate events due to global warming, the methods and findings from this study can be further used and developed for coastal monitoring purposes in coming years, in association with other data sources.

1. Introduction

In the context of global warming and climate change, sea waves play a key role in shaping human and environmental risks in coastal and port areas. Globally, Reguero et al. (2019) estimated Wave Power (hereafter WP), a parameter used to characterize energy transfer and long-period wave behavior. WP measures (over cumulative periods of time) the transmission of energy by air-sea exchanges and is employed for wave motion (Reguero et al., 2019). They also explored relationships between the WP and the upper ocean sea surface temperature (SST). Analyzing WP trends for the oceans from 1948 to 2008 the authors retrieve an increasing WP global trend of approximately 0.4% per year over this interval and note that global WP and SST are strongly associated. Wave power trends in regional seas (e.g., Caloireo et al., 2019; Saprykina et al., 2019; Vega et al., 2020) have particular importance for regions of high population density and extensive coastal infrastructure. Caloiero et al. (2022)

computed the WP trend for the Mediterranean Sea, showing a general increase in the mean wave energy period (the period corresponding to the wave energy weighted average), especially in the Ionian Sea.

Sea waves transferring energy between the hydrosphere and solid Earth generate the most prominent and continuous, global seismic wavefield on the Earth, the microseism (e.g., Hasselmann, 1963; Longuet-Higgins, 1950). Microseism can be divided by spectral content and source mechanism (e.g., Haubrich & McCamy, 1969) into primary (hereafter PM), and secondary (hereafter SM), bands. The SM is subdivided here into SM and short period secondary microseism (SPSM). The PM has the same period as the causative ocean waves (13–20 s) and is generated by the energy transfer of oceanic waves tractions on the seafloor in coastal and near-coastal regions with depths of less than several hundred meters (Ardhuin et al., 2015; Hasselmann, 1963). The SM typically exceeds the PM by 10–20 dB (Ardhuin & Roland, 2012; Lepore & Grad, 2018; Longuet-Higgins, 1950; Oliver & Page, 1963; Ardhuin et al., 2015). It originates from interfering sea waves propagating in opposing directions. Interference produces standing gravity waves which in turn, cause a nonlinear pressure perturbation. This pressure perturbation generates seismic body and (predominantly) Rayleigh surface waves at the ocean floor. The global SM is excited across a frequency range (5–10 s) that is approximately twice that of the causative ocean waves. In some regions, SPSM is also notable at periods shorter than 5 s, as generated by the interaction between local and near-coastal short period waves (Bromirski et al., 2005; Dorman et al., 1993).

Multiple works have analyzed the relationships between microseism and sea conditions (Ardhuin et al., 2019; Aster et al., 2008, 2010, 2023; Bromirski et al., 1999; Cannata et al., 2019, 2020; Cutroneo et al., 2021; Ferretti et al., 2013, 2018; Guerin et al., 2022; Minio et al., 2023; Moschella et al., 2020). Bromirski et al. (1999) was the first work to analyze the microseism to predict Significant Wave Height (hereafter SWH), defined as the average height of the highest one-third of the individual waves in a record (Munk, 1944). Bromirski et al. (1999) developed an empirically derived seismic-to-wave transfer function, suitable for the California coast and demonstrated the ability to predict real-time SWH using microseism data recorded by one seismic station installed near the coastline using a wave buoy. Similarly, Ferretti et al. (2018) developed an algorithm, later updated by Cutroneo et al. (2021), able to predict SWH metrics using the microseism amplitude recorded by a set of seismic stations installed along the Ligurian coast (Italy). Anthony et al. (2015, 2017), Pratt et al. (2017), and Cannata et al. (2019), analyzed relationships between the microseism recorded in Antarctica and Antarctic Sea ice, examining how sea ice concentration inhibits microseism generation, particularly in the PM band. These works indirectly demonstrated the importance of ocean waves interacting with coastlines for PM generation.

Other authors, in the context of climate change, have focused on analyzing long seismic time series to resolve trends in specific microseism indices or energy (Aster et al., 2010, 2023; Grevemeyer et al., 2000; Stutzmann et al., 2009). For example, Grevemeyer et al. (2000) analyzed north-east Atlantic Ocean microseism recorded by a station near Hamburg (Germany), for 1954–1998. Using the Microseism Index, defined as the number of days per month affected by strong microseism. The results showed a significant index increase, with an average increment of 0.26 days per year over the time interval analyzed, with the highest values occurring after 1978. Aster et al. (2023) analyzed primary microseism (0.05–0.07 Hz) vertical component data recorded by 52 globally distributed stations from the late 1980s to August 2022 to assess global near-coastal wave amplitudes and energies. Assuming a proportional relationship between sea waves and microseism energy for small changes, this study found geographically correlated (3σ uncertainties) significant increases for 41 stations and decreases for 8 stations (predominantly in the northern and western Pacific Ocean regions). The global average energy trend from this study is 0.27 ± 0.03% per year for all data and 0.35 ± 0.04% per year for data since the beginning of the 21st century (3σ uncertainties).

The above studies highlight the utility of microseism amplitude proxy measurements to infer sea state variations across multiyear intervals.

Here, we analyze the seismic signal recorded by nine seismic stations installed in the Mediterranean region (Figure 1a and Table S1 in Supporting Information S1) for data between 1 January 1996–15 October 2023. Using methodologies similar to Aster et al. (2023), we measure microseism energy trends for this time period. The analysis includes the PM (0.05–0.07 Hz), SM (0.1–0.2 Hz), SPSM (0.2–0.4 Hz) bands, and a 'general' microseism band encompassing all of these frequencies (0.05–0.4 Hz) We also calculate WP and WP trends from wave hindcast data for specific sea areas near the seismic stations (black rectangles in Figure 1a) to explore the relationship between hindcast estimated WP and microseism energy. In addition, we use two seismic stations

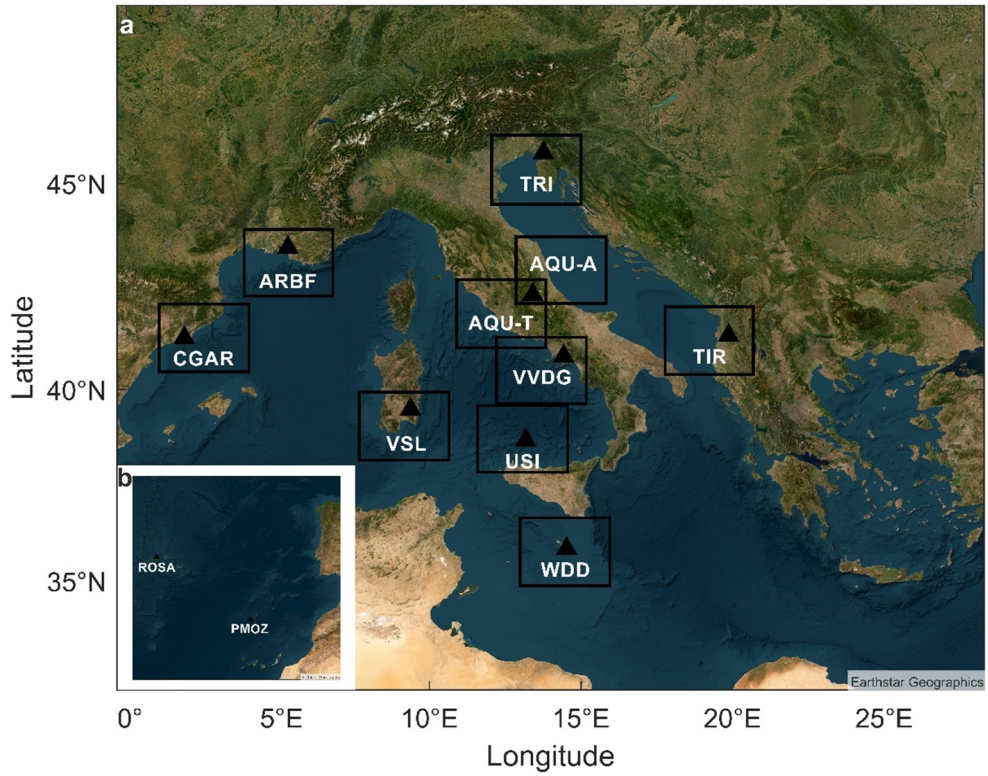

Figure 1. (a). Satellite image of the Mediterranean region with broadband seismic stations available in the ORFEUS and INGV databases used in our analysis. Black rectangles around the seismic stations represent the sea areas considered in the trend analysis. For the AQU seismic station two boxes were plotted (AQU-T refers to the box used for the Tyrrhenian Sea area, while AQU-A is for the Adriatic Sea); (b) map showing the portion of the Atlantic Ocean where the seismic stations PMOZ and ROSA are located (base images source ©Earthstar Geographic).

installed on the Madeira and Sao Jorge islands (Figure 1b) to compare Mediterranean and Atlantic Ocean microseism features, finding some differences.

2. Data and Methods

This work analyzes microseism and hindcast data for the period 1 January 1996–15 October 2023 as described below. The investigated period was constrained by the availability of seismic data.

2.1. Seismic Data

We used vertical component data recorded by nine Mediterranean seismic stations (Figure 1a and Table S1 in Supporting Information S1) installed in Italian (AQU, TRI, USI, VSL, and VVDG), Maltese (WDD), French (ARBF), Spanish (CGAR), and Albanese (TIR) coastal areas, and from two seismic stations installed on the Madeira (PMOZ) and Sao Jorge (ROSA) Islands in the Atlantic Ocean (Figure 1b). The selected seismic stations: (a) are installed in coastal areas, (b) are equipped with 3-component broadband (BHZ channels) or high broadband seismic sensors (HHZ channels); and (c) have long-duration seismic records. The BHZ channels, where available, have a sampling rate of 20 Hz and the HHZ channels have a sampling rate of 100 Hz. The number of available seismic stations varies across the years because of operational time period and/or technical failures. Four seismic stations (AQU, CGAR, VSL, and WDD) have data availabilities of greater than 75%, three (ARBF, TIR, and USI) are in the range of 50%–75% and two (TRI and VVDG) are below 50%. Since we considered a long-time interval and the seismic stations began operating at different times, and have intervals of inactivity, we need an accurate description of the operational times (start and end) and the duration of any malfunctions. A detailed description of each station's performance is given in Figure S1 in Supporting Information S1 and Table

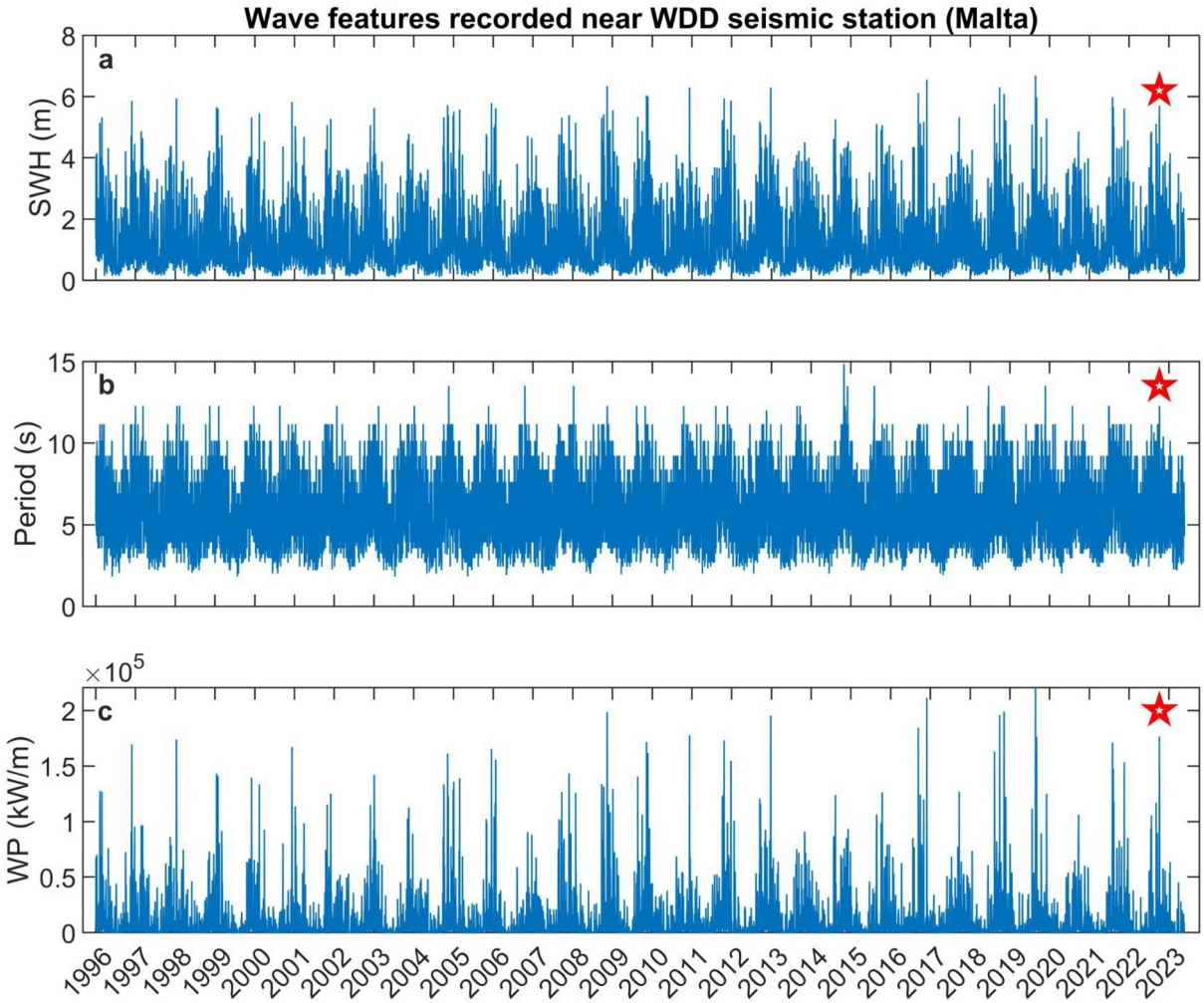

Figure 2. Significant Wave Height (SWH) (a), Period (*Tp*) (b), and Wave Power (WP) (c) obtained from the hindcast maps for the sea area around Malta (Figure 1). Red star represent the extreme value of SWH, Period and WP recorded during the sub-tropical system Helios (Borzì, Minio, De Plaen, Lecocq, Alparone, et al., 2024).

S1 in Supporting Information S1. The PMOZ and ROSA seismic stations used only to compare Atlantic and Mediterranean microseism features, began recording on 19 January 2009.

2.2. Sea Data

To gather hindcast estimates of sea state and WP, we utilized the MEDSEA_HINDCAST_WAV_006_012 dataset provided by the Copernicus Marine Environment Monitoring Service (CMEMS). The CMEMS product contains hindcast maps of the Mediterranean Sea Waves forecasting system and is based on the third-generation wave model WAM Cycle 4.5.4, composed of hourly wave parameters at 1/24° horizontal resolution (Korres et al., 2019). Hourly data on the SWH and peak period (hereafter *Tp*) were employed to reconstruct the sea state and WP. Examples of SWH, *Tp,* and WP time series are shown in Figure 2.

2.3. Seismic Data Analysis

The seismic data were corrected for instrument response to velocity units (m/s) for spectral and amplitude analyses. Welch's method (Welch, 1967) was applied to estimate power spectral densities (PSDs), using non-overlapping time windows length of 81.92 s, averaged over 1 hour to obtain hourly spectra. Hourly PSD estimates were gathered and visually evaluated as spectrograms, in frequency versus time using a $\log_{10}$(PSD) color scale. Figure 3 displays spectrograms for the vertical components of the seismic stations used in this study.

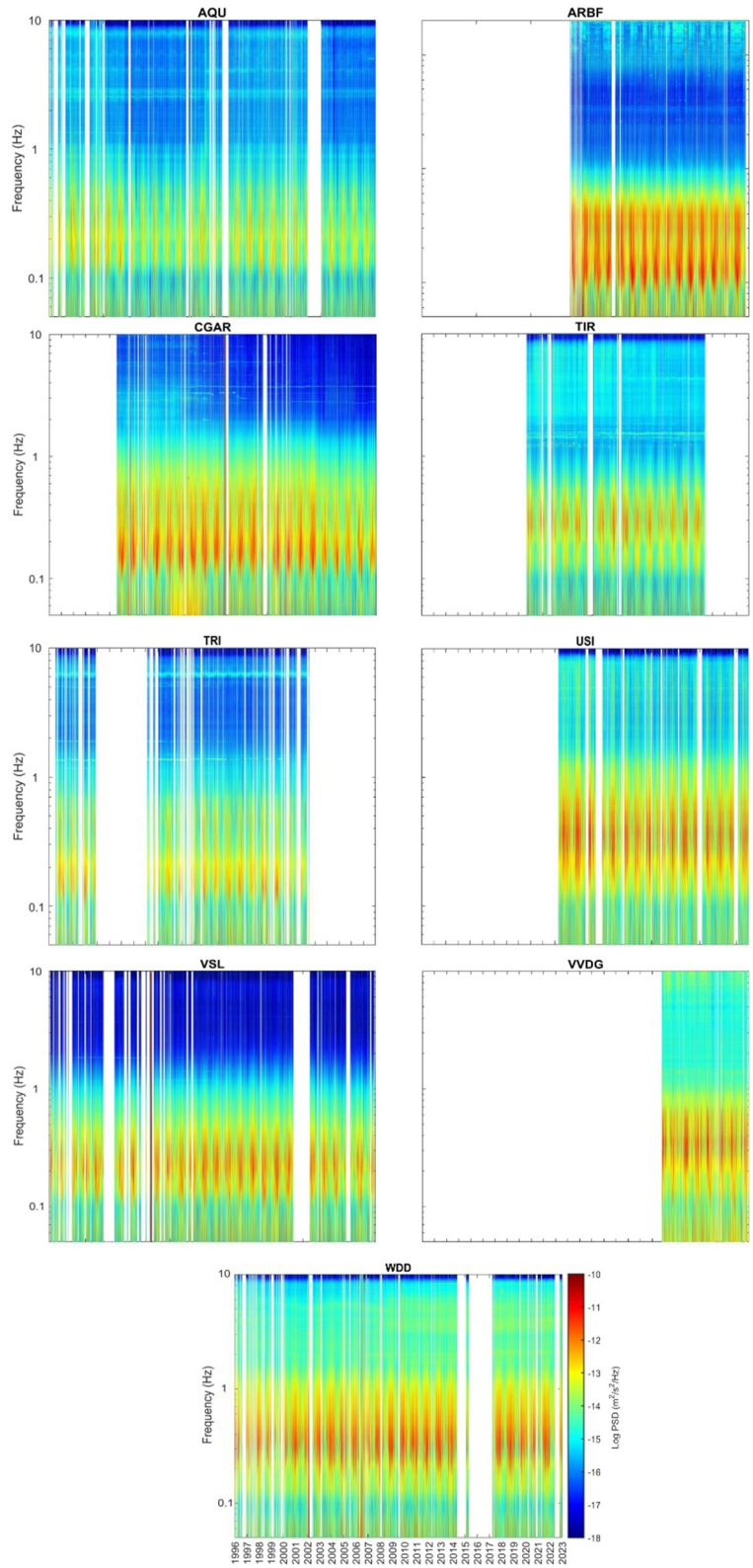

Figure 3. Power spectral density spectrograms of vertical seismic velocity for the nine stations of Figure 1a.

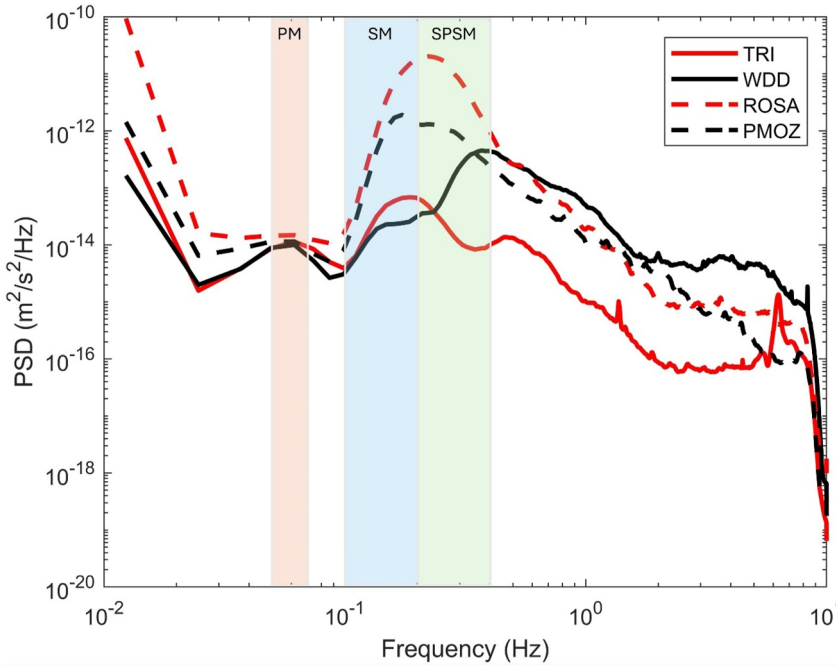

Figure 4. Median spectra of two Mediterranean seismic stations (red and black continues lines) and of two Atlantic seismic stations (red and black dashed lines).

For the specific microseism frequency bands of 0.05–0.07 Hz (PM), 0.1–0.2 Hz (SM), and 0.2–0.4 Hz (SPSM) we computed hourly root mean square (RMS) amplitude time series. An RMS amplitude time series was also retrieved for the "general" microseism band (0.05–0.4 Hz) spanning all aforementioned frequency bands. To estimate microseism energy, we square the RMS seismic velocity values and refer to this parameter as Microseism Squared Amplitude (hereafter MSA).

In addition, the median spectra for the stations WDD, PMOZ, ROSA, and TRI, calculated for the data recorded during the interval 19 January 2009–04 August 2017 (corresponding with the interval when all the data recorded by these stations were available), are plotted in Figure 4. An example of PSD from the probability density function for the same stations is plotted in Figure S2 in Supporting Information S1.

Finally, to compile a catalog of the greater extreme meteo-marine events affecting the Mediterranean Sea during the period under consideration, we looked for common peaks within the RMS amplitude time series of the analyzed stations. In particular, we: (a) synchronized the daily RMS amplitude time series obtained from the different stations, (b) deleted the outliers (such as electronic noises and earthquakes) by removing the RMS amplitude values greater than 99.9 percentile, (c) normalized the RMS amplitude time series by dividing each time series by its maximum value; (d) calculated the median among time-coincident RMS amplitude values at different stations, (e) considered the six highest peaks of the median time series. Since the RMS amplitude at each station can be influenced by factors such as the distance between the source and station, geology, and site effects, we chose to normalize the RMS amplitude time series (step c) for comparison. For the same reason, we decided not to consider extreme events at every single station but at most of the stations, hence the selected extreme events are the ones able to affect the entire Mediterranean Sea or at least a large portion of it. Consequently, only peaks from periods when at least 6 out of 9 stations properly recorded data were considered. This threshold started to be almost continuously reached from 2004 onwards, and for this reason, the retrieved extreme meteo-marine events fall within the time interval 2004–2023.

2.4. Correlation Analysis Between Sea State and Seismic RMS Amplitude

We calculated correlation coefficients between the seismic RMS amplitude time series (for each microseism band in this study) and for the SWH time series, following the methodologies used in Bromirski (2001) and Borzì, Minio, De Plaen, Lecocq, Alparone, et al. (2024). To assess correlation coefficient spatial variability, this

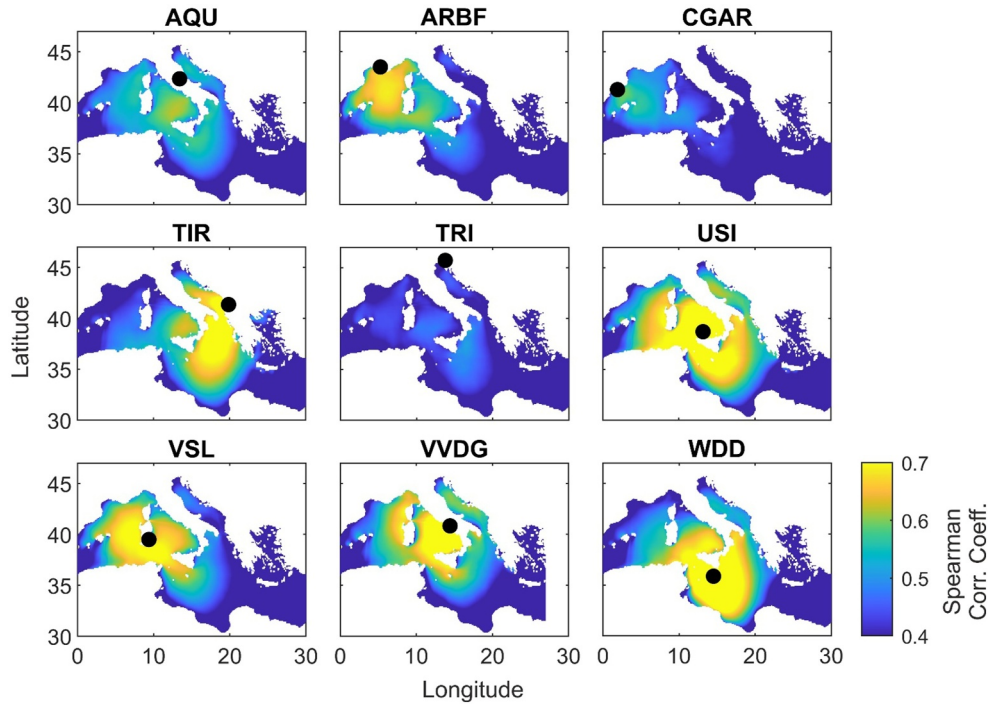

Figure 5. Correlation maps obtained for the vertical component of each station between the microseism band (0.05–0.4 Hz) and the SWH for the entire station operational period (see Figure S1 in Supporting Information S1). Black dots indicate the position of the seismic station.

calculation was performed for each grid cell of the hindcast maps for the entire period of this study. Such an analysis offers insights into the principal sources of microseism activity recorded by all nine stations.

To investigate the relationship between seismic RMS amplitudes and SWH, we adopted the approach introduced by Craig et al. (2016) using the Spearman correlation coefficient, a non-parametric measure of the rank correlation. Correlation value contour maps were generated for each node of the grid covering entirely the Mediterranean Sea (1890 km × 2690 km, Figure 5 and Figure S3, S4, and S5 in Supporting Information S1) for the vertical component of each station and for both the general microseism frequency bands (Figure 5) and for the typical microseism frequency bands (PM in Figure S3 in Supporting Information S1, SM in Figure S4 in Supporting Information S1 and SPSM in Figure S5 in Supporting Information S1). In addition, we also plotted the Spearman correlation coefficient, computed between the RMS amplitude time series of the general microseism band and the SWH, against the distance between the seismic station and the sea grid cell to estimate the portion of the sea that affected the microseism amplitude (Figure 6).

Finally, to explore the temporal variability and potential seasonality we calculated the Spearman correlation coefficient between the RMS amplitude (for all the microseism bands: PM, SM, SPSM, and the general microseism band), and for the SWH time series for each sea area and station in this study. Since SWH is expressed as a three-dimensional grid (latitude, longitude, and time) we calculated the spatial SWH median to obtain an SWH time series for each sea area and subsequently estimated the Spearman correlation coefficient time series. To perform this analysis, we used a 30-day long moving window with a 1-day step (overlap of about 96%).

2.5. Sea Data Analysis

To identify the sea regions most responsible for the microseism signals at each station we selected a sea area with an extent of 4650 km^2 centered around the seismic station location (black rectangles in Figure 1a). In the case of station AQU, two areas were encompassed since this station lies halfway between the Adriatic and the Tyrrhenian Seas.

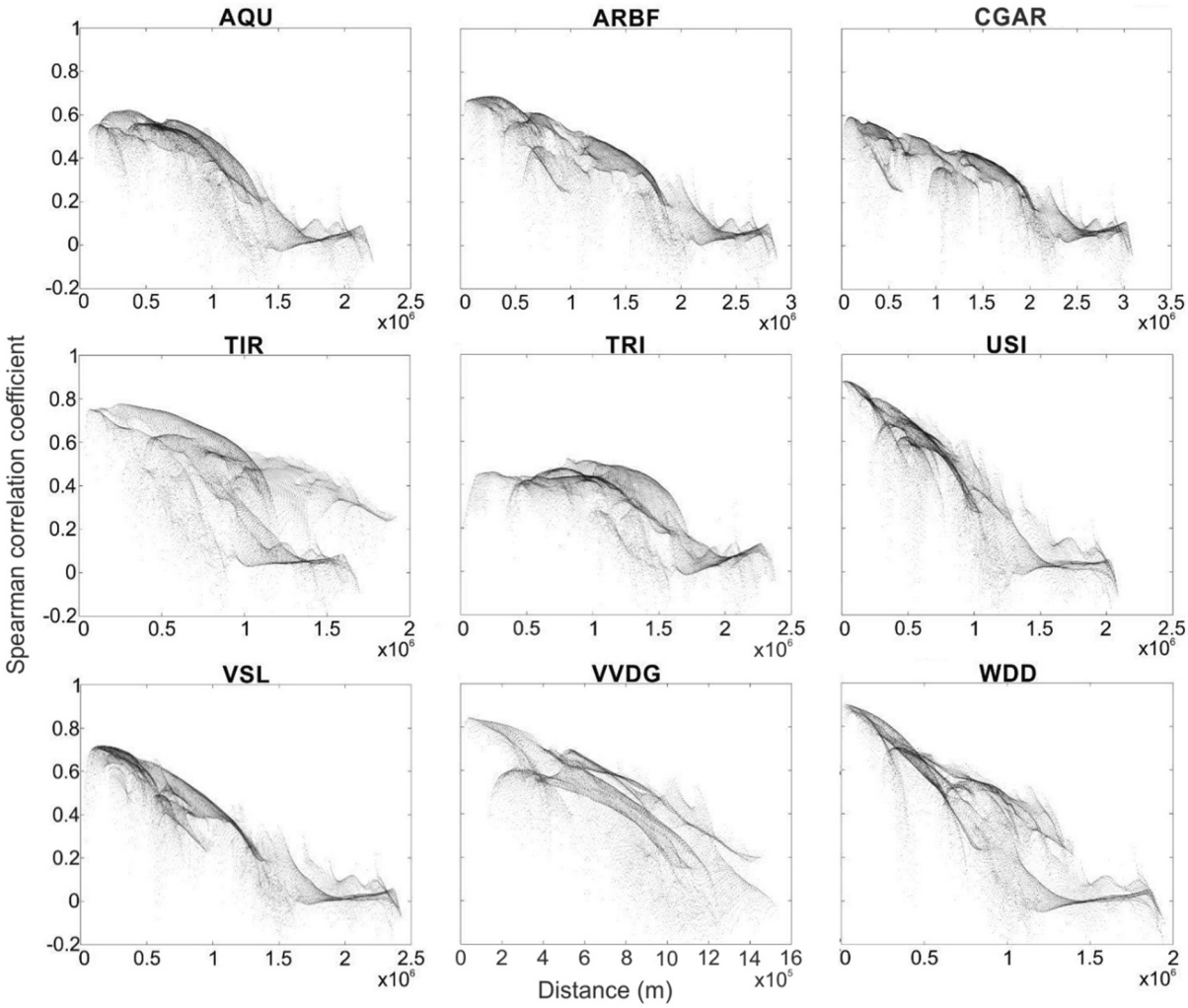

Figure 6. Spearman's correlation coefficient, computed between SWH and seismic RMS amplitudes for the general microseism frequency band (0.05–0.4 Hz) as a function of distance between the seismic station and each sea grid cell.

Within these selected areas we obtained the hourly SWH and *Tp* for each node of the two-dimensional grid for the full study time period using the MEDSEA_HINDCAST_WAV_006_012 dataset. To obtain daily SWH and *Tp* time series, we computed the daily median within the area of each grid node.

To parameterize wave behavior, several authors (e.g., Caloiero & Aristodemo, 2021; Reguero et al., 2019) have employed WP parameters. When SWH and *Tp* data are available, *WP* can be calculated according to (Amrutha & Sanil Kumar, 2016)

$$W_P = \frac{\rho g^2}{64\pi} T_e (H_s)^2 \quad (1)$$

where WP is computed in kW/m, ρ is the seawater density (influenced by salinity and temperature; in this study, an average value of 1025 kg/m^3 is adopted), g is the acceleration of gravity (9.81 m/s^2), H_s is the SWH (m), and T_e is energy period (s). The energy period can commonly be estimated from the peak period as $T_e = 0.9T_p$ (Amrutha & Sanil Kumar, 2016).

Using SWH and *Tp* we computed hourly and daily WP for each sea area across the study period.

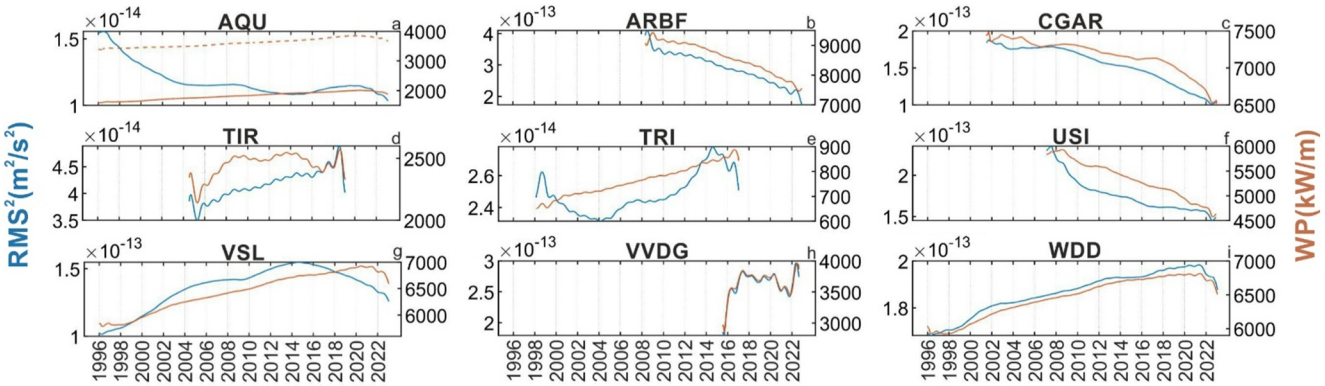

Figure 7. Long-term trends obtained from SSA analysis for each station and their corresponding sea areas. The light blue line represents the long-term SSA trend obtained using the seismic data, while the orange one represents the long-term trend obtained using the sea data. In the AQU case (a), the dashed orange line represents the WP trend obtained for the Tyrrhenian Sea area, while the orange line represents the WP trend of the Adriatic Sea area.

2.6. Singular Spectrum Analysis Trend

To analyze variations in MSA for the general microseism band and WP during the study period we used Singular Spectrum Analysis (hereafter SSA; Golyandina et al., 2013). SSA analysis has also been used to analyze other geosciences fields. For example, Dumont et al. (2020) used SSA to study the seismic tremor and power radiated by the lava field and their relationship with the Sun-Moon gravitational forces, during the Holuhraun eruption (Iceland). For a uniformly sampled time series the SSA algorithms partition the data into (a) Long-term Trend (LT), (b) Seasonal or oscillatory Trend (ST), and (c) Remainder (*R*). So that the original time series is composed of the sum of LT, ST, and *R*. We first remove the outliers (including teleseismic earthquakes) and analyze daily MSA and daily WP time series to estimate LT (Figure 7), ST (Figure S6 in Supporting Information S1), and the *R*. To characterize daily WP and MSA, we compute the median value for 24 hr. We also computed the Spearman correlation coefficient between the long-term trend for the WP and MSA to examine the relationship between these two datasets.

The sea data at our disposal does not have a sufficient resolution to allow us to distinguish coastal areas from open sea areas, especially for island regions (such as Ustica or Malta; see Figure S1 in Supporting Information S1) where sea depths can rapidly vary. As explained in the literature (e.g., Bromirski et al., 2005), microseism generation is strongly affected by the sea depth. PM is generated only in shallow waters and where the depths are less than approximately ½ λ (where λ is the wavelength of the ocean waves) while SM can be generated also in open seas and is strongly influenced by water column resonance. Hence, we chose to analyze the MSA trend for the general microseism band since this includes the signal generated by different source mechanisms and can be compared with the WP trend calculated for the whole area. In addition, this confirms that the greater part of the general microseism band is dominated by the SM and SPSM bands with little contribution from the (much lower power) PM band.

3. Results and Discussion

In this work, we analyzed a multi-decadal time series (1 January 1996–15 October 2023) of sea wave parameters and multi-band microseism data. For the sea wave data, we used the WP parameter, and for the microseism, we employed the MSA, which is proportional to seismic signal energy. In addition, we retrieve the long-term trends and other SSA information from these two datasets to verify if the considered parameters show a relationship during the specified time interval.

3.1. Sea State and Wave Power

Using the MEDSEA_HINDCAST_WAV_006_012 dataset, we retrieved hourly SWH and *Tp* values and calculated their daily medians for each area. In Figure 2 we plot an example of daily SWH, *Tp,* and WP obtained for the area around the seismic station WDD installed in Malta. As expected, seasonal modulation of these three parameters is evident with greater values of SWH, *Tp,* and WP during the autumn and winter months and lower

Table 1
Catalog of the Greatest Extreme Events Recorded in the Mediterranean Sea During the Period Under Consideration

Name	Date	Normalized amplitude values	SWH max (m)	Area with SWH>3 m (km^2)
Storm 1 (Vaia)	29/10/2018	0.401	7.45	851,740
Storm 2	23/12/2019	0.395	7.63	954,270
Storm 3	14/12/2019	0.382	7.91	874,530
Storm 4	06/02/2013	0.374	4.55	285,410
Storm 5	12/02/2014	0.368	4.62	226,350
Storm 6	18/02/2009	0.365	4.97	174,840

during spring and summer. Similar results, in terms of seasonality, for the other considered sea areas were observed. Peaks occurred during extreme weather events, such as the sub-tropical system Helios (early February 2023), when SWH reached approximately 6 m, *Tp* about 12 s, and WP exceeded 1.5×10^5 kW/m (red star in Figure 2).

3.2. Spectral and Correlation Analysis

In Figure 3 we plot $\log_{10}$ (PSD) spectrograms for vertical component seismic velocity. As highlighted by several authors studying relationships between microseism and the sea waves in the Mediterranean area (Borzì, Minio, De Plaen, Lecocq, Alparone, et al., 2024; Borzì, Minio, De Plaen, Lecocq, Cannavò, et al., 2024; Borzì et al., 2022; Cannata et al., 2019, 2020; Cutroneo et al., 2021; Ferretti et al., 2013, 2018; Minio et al., 2023; Moschella et al., 2020) and in the oceans more generally (Ardhuin et al., 2019; Aster et al., 2008, 2010, 2023; Bromirski, 2001; Bromirski et al., 2005; Gerstoft et al., 2006; Gualtieri et al., 2018; Lin et al., 2017; Retailleau & Gualtieri, 2019, 2021; Zhang et al., 2010), these spectrograms show that a great part of the energy is focused at 0.1–1 Hz, corresponding to the SM and SPSM bands, reflecting the relatively high seismic efficiency of the SM process relative to the PM. Figure 3 also displays microseism seasonality, highlighted by annually alternating high and low PSD values. As noted by other authors (e.g., Shabtian et al., 2023; Stutzmann et al., 2009), the strong microseism seasonal modulation at mid-to-high latitudes is due to seasonal different meteorological conditions at temperate latitudes, especially the occurrence of large extratropical cyclonic storm systems, with higher northern hemisphere microseism PSD values obtained during the autumn and winter months (typically from September to March) and lower PSD values during the spring and summer months (typically from April to August). Indeed, during the autumn and winter months in the Mediterranean area, more powerful meteorological phenomena such as storm surges, Atlantic perturbations, sub-tropical cyclones, and Medicanes, take place. These phenomena generate sea storms producing higher seismic noise levels in microseism bands because of the energy transfer from sea waves to the solid Earth. Similar results are observed for the RMS amplitude time series of all microseism bands (Figure S7 in Supporting Information S1). In Figure S7 in Supporting Information S1, as an example, we plot the RMS amplitude time series for station WDD for the four microseism bands: PM (0.05–0.07 Hz), SM (0.1–0.2 Hz), SPSM (0.2–0.4) and general microseism band (0.05–0.4 Hz). As in the spectrogram case, it is clear the seasonal modulation of the RMS amplitude with peaks during the autumn-winter months and lower values during the spring-summer ones. In Figure S8 in Supporting Information S1 we plotted the microseism RMS amplitude (in the general microseism band) for the WDD station, and the period, SWH, and WP time series for the corresponding sea area during 2020 to display the variation of these parameters during a single year. We chose this year because it showed a high continuity of the seismic signal. The RMS amplitude, SWH (Figure S8a in Supporting Information S1), and WP (Figure S8c in Supporting Information S1) variations are in phase. In contrast, the relationship with the period (Figure S8b in Supporting Information S1) is less evident. This is confirmed by the Spearman correlation coefficient calculated between the RMS-SWH (0.89), RMS-Period (0.67), and RMS-WP (0.92) time series.

Finally, we compiled a catalog of extreme meteo-marine events by considering the first six events that show the greatest RMS amplitude values. In Table 1 we reported the extreme events obtained by performing this analysis, along with the extent of the sea area affected by SWH greater than 3 m, which, as discussed by Borzì, Minio, De Plaen, Lecocq, Cannavò, et al. (2024), represents the SWH threshold for a significant increase in the RMS amplitude. Similar to the results obtained by Borzì, Minio, De Plaen, Lecocq, Cannavò, et al. (2024), microseism amplitude is strongly related to the sea area affected by SWH greater than 3 m. In addition, meteorological events

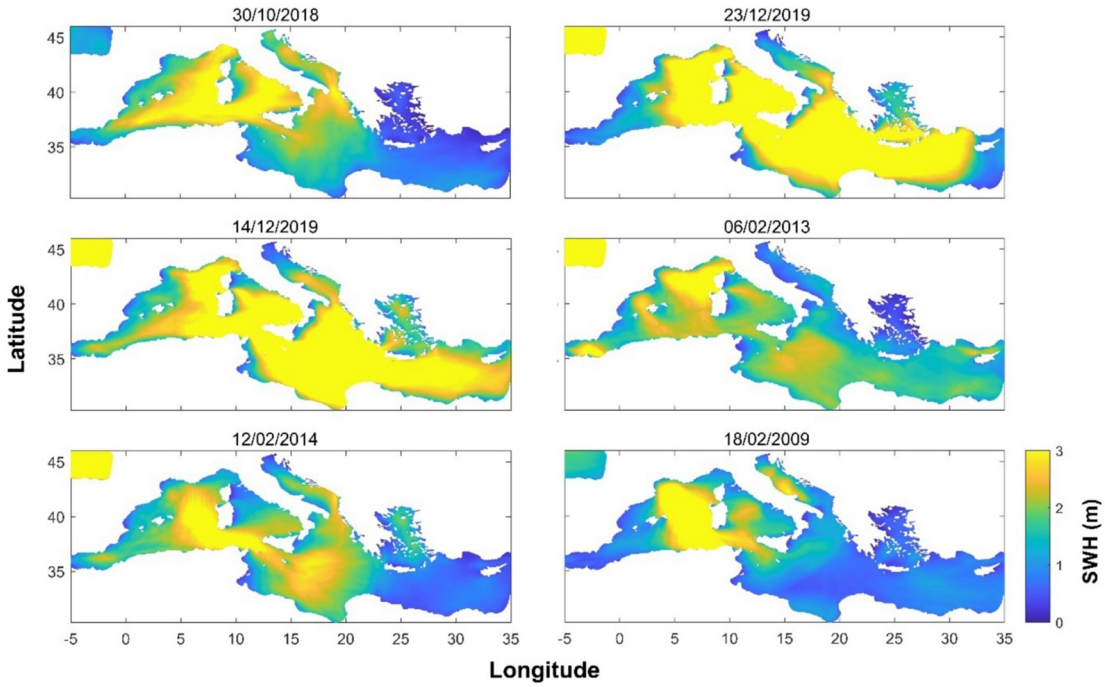

Figure 8. Hindcast maps showing the SWH recorded during the greatest extreme events that occurred in the Mediterranean area during the period under consideration.

that generate greater seismic amplitude are Atlantic perturbations rather than Medicanes since the latter are spatially more limited. The highest normalized amplitude was obtained during the "Vaia" storm, an extreme event that occurred between 28 and 30 October 2018 and was able to produce severe damage to northern Italy's forests as well as storm surges along the Italian coasts (Figure 8; Vaglio Laurin et al., 2021).

For each station, we calculate the Spearman correlation coefficient between the RMS amplitude time series for the microseism bands in this study (0.05–0.07, 0.1–0.2, 0.2–0.4 and 0.05–0.4 Hz) and the SWH for the entirety of the Mediterranean Sea (Figure 5, Figure S3, S4 and S5 in Supporting Information S1 and Table 2). For the general microseism band (Figure 5), the seismic stations WDD, VVDG, VSL, USI, and TIR show the highest Spearman correlation coefficient (greater than 0.8), stations CGAR, AQU, and ARBF show a correlation coefficient in a range of 0.6–0.8, and station TRI shows the lowest correlation coefficient (∼0.5). All areas characterized by high correlation coefficient values show a strong inter-station spatial association with the exception of TRI. For WDD the region characterized by the highest Spearman correlation coefficient is the Sicily Channel and part of the

Table 2
Spearman Correlation Coefficients Obtained Between the RMS Amplitude and the SWH Time Series and Between the MSA and WP Trends Time Series

Considered sea area and seismic station	Highest spearman corr. Coeff. Among the SWH and RMS amplitude time series	Highest spearman corr. Coeff. Among the WP and MSA trends time series
AQU - Adriatic Sea	0.48	−0.81
AQU - Tyrrhenian Sea	0.62	−0.80
ARBF	0.70	0.91
CGAR	0.60	0.94
TIR	0.77	0.61
TRI	0.52	0.44
USI	0.87	0.96
VSL	0.72	0.70
VVDG	0.84	0.97
WDD	0.90	0.95

Ionian Sea. For stations USI, VSL, and VVDG the area characterized by the highest coefficient is the Tyrrhenian Sea, for ARBF and CGAR the highest correlation coefficient is in the western portion of the Sardinian and the Balearic Seas, respectively, while at TIR the area characterized by the highest correlation coefficient is the Ionian Sea and in a small portion of the Adriatic Sea (Figure 5). This demonstrates, in agreement with prior literature (Borzì, Minio, De Plaen, Lecocq, Alparone, et al., 2024; Craig et al., 2016; Minio et al., 2023), that the sea area that mostly affects the microseism amplitude at a given station across the Mediterranean is the one closest, with the exception of TRI.

Concerning the temporal variation or potential seasonality in the Spearman correlation coefficient, calculated between the seismic RMS amplitude, in the general microseism band, and SWH time series, our analyses show a fairly stable coefficient during the period taken into account for each seismic station and sea area analyzed in this study. As an example, in Figure S9 in Supporting Information S1 we plot time on the *x*-axis and the Spearman correlation coefficient on the *y*-axis for the entire period analyzed (a) and for 1 year (b) for the WDD station and corresponding sea area. By observing Figure S9a and S9b in Supporting Information S1 it is possible to note: (a) the absence of specific long-term trends or seasonal cycles and (b) occasional and randomly distributed outliers with very low correlation values, probably due to other seismic noise sources unrelated to microseism, or to station malfunctions. Finally, we calculated the median Spearman correlation coefficient (0.86) and its standard deviation (0.07) for the entire period considered, affirming the general stability of this parameter across the analyzed time interval.

Considering the typical microseism bands separately (PM in Figure S3 in Supporting Information S1, SM in Figure S4 in Supporting Information S1, and SPSM in Figure S5 in Supporting Information S1) the results show, as expected, that the microseism bands best correlated with the sea state and with the SWH are the SM (Figure S4 in Supporting Information S1) and, particularly, the SPSM (Figure S5 in Supporting Information S1). The results for the PM (Figure S3 in Supporting Information S1) show a lower Spearman correlation coefficient (0.2–0.4) than those for the SM and SPSM (note that the colorbars for the PM have a different scale with lower values than the other two cases). This evidence, along with the similar areal shapes retrieved for the areas characterized by higher Spearman correlation coefficient observed in Figure 5 (general microseism band) and Figure S5 in Supporting Information S1 allow us to infer that the microseism band which most influenced the Spearman correlation coefficient for the general microseism band is the SPSM band. Figure 6 shows the Spearman correlation coefficient computed between the SWH and the RMS amplitude of the general microseism band, with the distance between the seismic station and the sea grid cell indicated. All seismic stations except for TRI, show a similar trend characterized by a near-monotonic decrease in coefficient with increasing station-sea cell grid distance. The area characterized by the highest Spearman correlation coefficient, in agreement with Cannata et al. (2020), is located on average in the first 500 km from the coastline. For TRI, the area characterized by the highest correlation coefficient (even if this station shows the generally lowest value of Spearman correlation coefficient among the considered seismic stations) is the Ionian Sea and not the Adriatic Sea as would be expected (Figure 5). This is clear also in Figure 6 where the trend obtained for this station is different from the others, showing an initial increase (from ∼0.4 to ∼0.5), followed by a decrease with increasing station-sea cell distance. The highest TRI correlation coefficient is obtained for a range of 1,000–1,500 km from the station, which corresponds to the distance between TRI station and the Ionian Sea. This could be explained by considering the typical sea state condition of the two seas. The Ionian Sea is usually stormier and rougher than the Adriatic Sea (Figure S10 in Supporting Information S1). We also calculate the standard deviation and the median value of SWH and WP for the two considered seas. The Ionian Sea shows higher values of both standard deviation and median computed on SWH data (0.76 and 0.86 m for the Ionian Sea and 0.46 and 0.52 m for the Adriatic Sea), Te data (1.30 and 5.15 s for the Ionian Sea and 1.19 and 3.87 s for the Adriatic Sea) and WP data (1.14×10^4 kW/m and 1.84×10^3 kW/m for the Ionian Sea and 3.31×10^3 kW/m and 5.46×10^2 kW/m for the Adriatic Sea). In addition, the TRI seismic station may be affected by the microseism generated from the Atlantic Ocean, which represents a stronger source than the Adriatic Sea. For example, Retailleau et al. (2017) used a set of seismic stations, installed also in Austria and Italy to locate Atlantic microseism sources, testifying that these seismic stations detect microseism energy generated by the Atlantic Ocean. To investigate whether the microseism signal recorded at the TRI station is influenced by Atlantic microseisms, we compared the median spectra of TRI, WDD, ROSA, and PMOZ in Figure 4, based on data from 19 January 2009–4 August 2017. We chose these stations since WDD can be considered (Figure 5) as a representative of the central Mediterranean Sea, TRI is the "outlier" among the Mediterranean seismic stations analyzed, and PMOZ and ROSA are the two Atlantic seismic stations

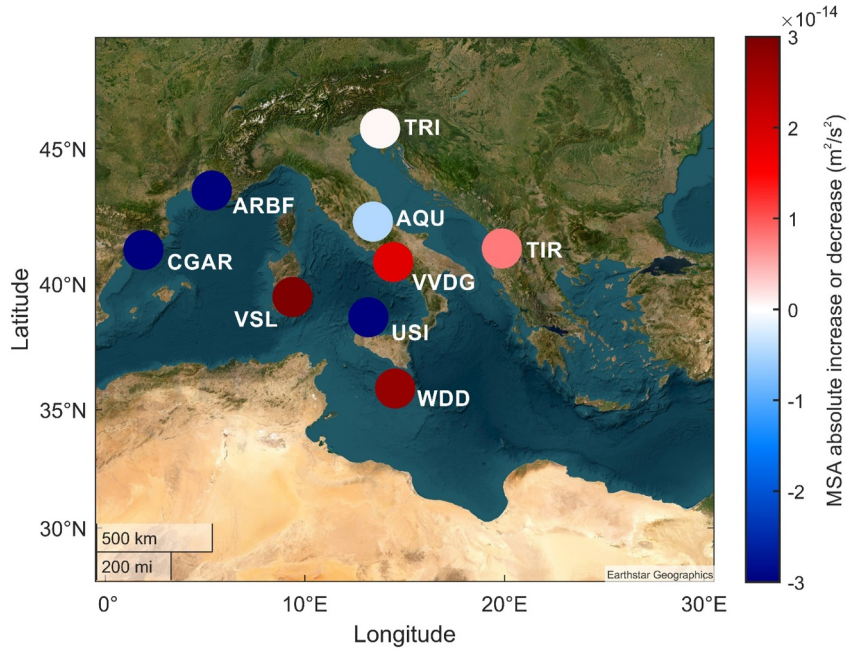

Figure 9. Maps of the Mediterranean area showing the MSA absolute increase or decrease recorded for each station. Each dot represents a seismic station and the color the variation in MSA as shown by the colorbar.

used to compare Mediterranean and Atlantic microseism. Observing Figure 4 TRI and WDD spectra show microseism peaks at different frequencies. TRI microseism peaks best agree with the (lower frequency) Atlantic microseism peaks (ROSA and PMOZ) while WDD peaks occur at higher frequency as previously noted in the literature (e.g., Becker et al., 2020; Janiszewski et al., 2023), that the shorter wave periods microseism characteristically occur in closed basins compared to the oceans.

3.3. Singular Spectrum Analysis Trends

A principal goal of this work is to assess variations in the MSA and WP and, specifically, their correlation during the period 1996–2023.

We analyze seismic and wave data using an SSA approach to obtain the long-term trend (Figures 7 and 9; Table 3) and the seasonal or oscillatory trends (Figure S6 in Supporting Information S1). A representative example of the results of the seasonal trend analysis for the WDD seismic station and sea area, plotted in Figure S6 in Supporting Information S1, shows a near-sine wave with annual periodicity peaking in late-autumn and winter months and having minima corresponding to spring and summer months for both MSA (Figure S6a in Supporting Information S1) and WP (Figure S6b in Supporting Information S1). In Figure 7, the results of the long-term trend of both MSA (light blue) and WP (orange) obtained for each seismic station and sea area are plotted.

Although the focus of this work is not trend analysis but is, rather, to demonstrate that the microseism data can be useful in long-term sea state analysis, we provide an overview of the main findings from SSA analysis. In particular, we observe increasing trends in both MSA and WP retrieved for four seismic stations and sea areas (TIR, VSL, VVDG, and WDD in Figures 7d–7g and 7h, 7i; Figure 9; Table 3), decreasing trends for three stations (ARBF, CGAR and USI in Figure 7b, 7c, 7f; Figure 9; Table 3) and stable trends retrieved for two stations (AQU and TRI in Figures 7a and 7e, 9 and Table 3). The WP trend retrieved for AQU and TRI (Table 3) shows elevated values of relative increase (0.8% per year and 1.51% per year, respectively) but the absolute values of WP are among the smallest obtained values (especially in the TRI case). WP and MSA trends show an excellent agreement for all areas except in the AQU and TRI cases. ARBF, CGAR, and USI (Figure 7b, 7c, 7f; Table 3) show a decreasing trend for both WP and MSA. TIR, VSL, VVDG and WDD (Figures 7d–7g and 7h, 7i; Table 3) show an increasing trend for both the parameters while, in AQU and TRI, these two parameters seem to be uncorrelated. To quantify the correlation among these two parameters we calculate the Spearman correlation

Table 3
Absolute and Relative Trend Increases or Decreases for WP and MSA

Considered sea area and seismic station	WP relative increase or decrease (%/yr)	WP absolute increase or decrease (kW/m)	MSA relative increase or decrease (%/yr)	MSA absolute increase or decrease (m^2/s^2)	Start date	End date	Duration of operational period (years)
AQU - Adriatic Sea	0.51	369.83	−0.9	−4.46e−15	01/01/1996	15/10/2023	27
AQU - Tyrrhenian Sea	0.40	378.31					
ARBF	−1.94	−2422.31	−3.53	−1.92e−13	04/09/2008	20/09/2023	15
CGAR	−0.48	−724.28	−2.51	−7.75e−14	27/08/2001	19/09/2023	22
TIR	0.47	334.02	0.41	7.75e−15	08/10/2004	12/09/2019	15
TRI	1.51	219.56	0.15	5.92e−16	18/03/1998	04/08/2017	19
USI	−1.35	−1088.41	−1.54	−7.68e−14	13/06/2007	21/08/2023	16
VSL	0.67	766.48	1.07	3.02e−14	01/01/1996	15/10/2023	27
VVDG	1.34	352.64	1.42	1.85e−14	20/01/2016	09/05/2023	7
WDD	0.49	802.62	0.57	2.72e−14	01/01/1996	15/10/2023	27

coefficient between the MSA and WP time series. Five stations show a Spearman correlation coefficient higher than 0.9 (ARBF, CGAR, USI, VVDG and WDD), two stations have coefficient in the range of 0.6–0.7 (TIR and VSL), TRI has a correlation coefficient of 0.44, and AQU has an anticorrelation for both the considered sea areas (−0.81 for the Adriatic Sea and −0.8 for the Tyrrhenian Sea). Spearman correlation coefficients are presented in Table 2. As in the case of the correlation analysis between the SWH and the RMS amplitude time series, the results of the trend analysis show a strong relationship between microseism and the sea state, particularly as characterized using WP. The results confirm that an increase (or a decrease) in the energy of the waves in the most proximal seas (estimated using WP) is reflected in an increase (or a decrease) in the MSA. This relationship is true for all the considered cases except, as seen above, for the more distal sensitivities observed at the AQU and TRI seismic stations and the corresponding sea areas. The higher Spearman correlation coefficient between MSA and WP was obtained, as expected, for the seismic stations installed closest to coasts (ARBF, CGAR, and VVDG) and on islands (WDD and USI). For the TRI case, the low correlation between WP and MSA time series could be linked to the stormier behavior of the more distant Ionian Sea compared to the Adriatic Sea, as highlighted in the Spectral and Correlation analysis section. Additionally, as discussed above, this low correlation may also be influenced by contamination from Atlantic microseism sources, as suggested by comparing the spectra of the Mediterranean (WDD) with those of the Atlantic (PMOZ and ROSA). The anticorrelation obtained for the AQU seismic station and the two selected sea areas (Adriatic and Tyrrhenian Sea) could be related to the relatively large distance between the seismic station and the two Italian coasts (~70 km AQU-Adriatic Sea and ~120 km AQU-Tyrrhenian Sea) and because nearest one is, generally, a calmer sea than the other. Trends obtained for the WP and the MSA of AQU and TRI show little variations during the analyzed 27 years. Considering AQU, the variation in Adriatic Sea WP (orange line in Figure 7a) and Tyrrhenian Sea (dashed orange line in Figure 7a) trends is less than 400 kW/m (Table 1), and the variations in MSA trend is lower than -4.5×10^{-14} m^2/s^2 (Table 3), while, considering TRI, the MSA variation is only -5.92×10^{-16} m^2/s^2 (Table 3) and the WP variation is less than 250 kW/m (Table 3). Given the small WP variations in these cases, the Adriatic Sea's generally lower energy state, and the distance between the AQU station and the coast, it is likely that the seismic stations could not resolve these minor WP variations.

Estimates trends and future trend scenarios are much debated in the literature and De Leo et al. (2024) highlighted this aspect. In particular, the complexity of the Mediterranean area, the multitude of sea wave models available, and the fact that analyses are based on these models and not on empirical data do not provide a full view of current

sea features (SWH and WP specifically) and their trends. Despite this, some regional trends show consensus in the literature. For example, both De Leo et al. (2024) and Rusu (2024) report that the Alboran Sea (western Mediterranean basin) shows positive trends in SWH and WP. Additionally, Rusu (2024) notes that this positive trend is also visible in the Adriatic and Aegean Sea. Finally, Caloiero et al. (2022) observe that the Ionian Sea also shows positive trends. Unfortunately, most seismic stations used in this study are installed far from these areas except for the station TIR (Adriatic Sea) and partially WDD (Sicily Channel-Ionian Sea). The MSA and WP increasing trends retrieved from our analysis confirm prior findings (Caloiero et al., 2022; Rusu, 2024). However, the most interesting finding from our analysis does not concern the WP and MSA trend results, which as mentioned above are the subject of debate within the oceanographic scientific community with conflicting views, but that the seismic stations and particularly the microseism have utility for long-term sea waves analysis. Indeed, as above mentioned, a great part of the analysis of sea wave trends is performed by using modeled sea data; also, our analysis of the SWH and WP makes use of hindcast data that essentially are revised modeled data. In contrast to hindcast data, MSA trends, and microseism amplitude variations are empirically derived directly from seismic recordings. Hence, the evidence found in this work (high correlation between MSA and WP), the agreement between our findings and the literature ones (the increasing trend in the Adriatic and Ionian Seas), and the increases in seismic data availability allow us to consider microseism as a complementary tool to investigate sea features.

4. Conclusions

Multiple studies have definitively demonstrated the strong relationships between microseisms and sea state (e.g., Ardhuin et al., 2019; Aster et al., 2008, 2010; Bromirski et al., 1999; Cannata et al., 2019, 2020; Cutroneo et al., 2021; Ferretti et al., 2013, 2018; Guerin et al., 2022; Minio et al., 2023; Moschella et al., 2020). In some cases, long seismic records have been analyzed to identify significant trends in specific microseism indices or MSA over multidecadal periods (Aster et al., 2010, 2023; Grevemeyer et al., 2000; Stutzmann et al., 2009). We performed an integrative analysis of seismic data recorded from 1 January 1996 through to 15 October 2023 for nine Mediterranean seismic stations with sea state data retrieved from CMEMS hindcast data. Two additional Atlantic seismic stations were included to compare Mediterranean and Atlantic microseism spectra. Spectral analysis results confirm strong seasonality in seismic signals, with higher amplitudes during stormy seasons and lower values in summer, as shown in prior work (e.g., Shabtian et al., 2023; Stutzmann et al., 2009) and characteristic of mid-to high-latitude seismic stations (e.g., Aster et al., 2008).

Correlation analysis between microseism amplitude and SWH time series shows that sea areas with the highest Spearman correlation coefficients are generally those that are nearest to each seismic station, except for TRI. Indeed, as confirmed by the Mediterranean and Atlantic spectrum comparison, signals from TRI may be influenced by Atlantic microseisms and also reflect the relatively high storminess of the more distal Ionian sea. Plotting the correlation coefficient against distance, source areas are shown to extend, on average, for about 500 km from the coastline (Figure 6), consistent with the results obtained by Cannata et al. (2020). As previously demonstrated in other works (Borzì, Minio, De Plaen, Lecocq, Alparone, et al., 2024; Bromirski et al., 1999; Craig et al., 2016; Minio et al., 2023), results confirm that secondary microseism amplitudes in the Mediterranean have the greatest sensitivity to the sea state within 500 km of the station. Using the SSA algorithm, we retrieve the long-term trends and the seasonality for the MSA and WP for each seismic station and nearby sea region, respectively. We find increasing long-term trends for both MSA and WP for four seismic stations and sea areas (TIR, VSL, VVDG and WDD), decreasing trends for three seismic stations and sea areas (ARBF, CGAR and USI), and stable trends for the remaining two stations (AQU and TRI). The Spearman correlation coefficient between seismic and wave power exhibits a strong correlation between these parameters for 7 out of the 9 seismic stations and their corresponding sea areas.

Based on these results, we infer that the Ionian Sea, and Sicily Channel, consistent with other studies (e.g., Caloiero et al., 2022) are characterized by a clear and progressive increase in WP over the study period. The Adriatic Sea shows a stable or slight increase (Rusu, 2024), and the Sardinian Sea a decreasing trend. For the Tyrrhenian Sea, some portions are characterized by an increase in both the parameters analyzed and others show a decrease. MSA trends and microseism amplitude variations, empirically derived from seismic recordings, contain plenty of information on the long-term changes of the sea wave features.

The results found by comparing the Mediterranean and Atlantic Ocean microseism spectra, confirm that the Mediterranean microseism is distinctly characterized by greater energy at higher frequencies than the ocean, which could be explored in detail in further work. Other works dealing with the long-term trend of MSA (e.g., Aster et al., 2023) or specific microseism indices (Grevemeyer et al., 2000) only consider seismic data while in our case we integrated both seismic and hindcast-constrained sea state data. The small number of stations available for this study (nine) does not allow us to obtain more detailed or complete spatial statistics but this exploratory work demonstrates the complementary potential of microseism measurements and independent sea state estimates to constrain wave climate in the Mediterranean region. In particular, the corroborative WP and MSA results in this study, the consistency between our findings and prior literature, the increased number of seismic stations installed in the last 20 years, ever-increasing data types and data sharing, and motivations driven by climate change and sea wave hazards, support implementation and expansion of these methods to longer time intervals and with greater spatial resolution at the Mediterranean and global scale.

Data Availability Statement

The seismic data, in the miniseed format used in this study, can be downloaded using the EIDA and ORFEUS webservices (http://www.orfeus-eu.org/data/eida/), and belong to the CA (Institut Cartogràfic i Geològic de Catalunya, 1984), FR (Epos-France, 1995), IV (Istituto Nazionale di Geofisica e Vulcanologia, 2005), MN (MedNet Project Partner Institutions, 1990), and PM (Instituto Português do Mar e da Atmosfera, I.P., 2006) networks. All the seismic stations used in this study and their main features are reported in Table S1 in Supporting Information S1. The Significant Wave Heights and Wave period information can be obtained by downloading the "Medsea_multiyear_wav_006_012" product on Copernicus website (https://data.marine.copernicus.eu/product/MEDSEA_MULTIYEAR_WAV_006_012/services).

Acknowledgments

This research has been funded by the PRIN 2022 PNRR project titled "ARCHIMEDE - MultidisciplinARy approaCH to better define vulnerability and hazard of MEDicanEs along the Ionian coasts of Sicily" (code P2022MJKMA, CUP H53D23011380001, E53D23021980001, B53D23033690001, Principal Investigator Prof. G. Scicchitano). R.C.A. was supported by NSF award EAR 2422648. The A.M.B. Ph.D. fellowship is funded by the PON "Ricerca e Innovazione 2014–2020 Azione IV.5 - Dottorati su tematiche green." The authors thank the two anonymous reviewers the Associate Editor, and the Editor, Rachel Abercrombie, for their comments that helped improve our manuscript. Open access publishing facilitated by Universita degli Studi di Catania, as part of the Wiley - CRUI-CARE agreement.

References

Amrutha, M. M., & Sanil Kumar, V. (2016). Spatial and temporal variations of wave energy in the nearshore waters of the central west coast of India. *Annales Geophysicae*, *34*(12), 1197–1208. https://doi.org/10.5194/angeo-34-1197-2016

Anthony, R. E., Aster, R. C., & McGrath, D. (2017). Links between atmosphere, ocean, and cryosphere from two decades of microseism observations on the Antarctic Peninsula. *Journal of Geophysical Research: Earth Surface*, *122*(1), 153–166. https://doi.org/10.1002/2016jf004098

Anthony, R. E., Aster, R. C., Wiens, D., Nyblade, A., Anandakrishnan, S., Huerta, A., et al. (2015). The seismic noise environment of Antarctica. *Seismological Research Letters*, *86*(1), 89–100. https://doi.org/10.1785/0220140109

Ardhuin, F., Gualtieri, L., & Stutzmann, E. (2015). How ocean waves rock the Earth: Two mechanisms explain microseism with periods 3 to 300 s. *Geophysical Research Letters*, *42*(3), 765–772. https://doi.org/10.1002/2014GL062782

Ardhuin, F., & Roland, A. (2012). Coastal wave reflection, directional spread, and seismoacoustic noise sources. *Journal of Geophysical Research*, *117*(C11). https://doi.org/10.1029/2011JC007832

Ardhuin, F., Stopa, J. E., Chapron, B., Collard, F., Husson, R., Jensen, R. E., et al. (2019). Observing sea states. *Frontiers in Marine Science*, *124*. https://doi.org/10.3389/fmars.2019.00124

Aster, R. C., McNamara, D. E., & Bromirski, P. D. (2008). Multidecadal climate-induced variability in microseisms. *Seismological Research Letters*, *79*(2), 194–202. https://doi.org/10.1785/gssrl.79.2.194

Aster, R. C., McNamara, D. E., & Bromirski, P. D. (2010). Global trends in extremal microseism intensity. *Geophysical Research Letters*, *37*(14). https://doi.org/10.1029/2010gl043472

Aster, R. C., Ringler, A. T., Anthony, R. E., & Lee, T. A. (2023). Increasing ocean wave energy observed in Earth's seismic wavefield since the late 20th century. *Nature Communications*, *14*(1), 6984. https://doi.org/10.1038/s41467-023-42673-w

Becker, D., Cristiano, L., Peikert, J., Kruse, T., Dethof, F., Hadziioannou, C., & Meier, T. (2020). Temporal modulation of the local microseism in the North Sea. *Journal of Geophysical Research: Solid Earth*, *125*(10), e2020JB019770. https://doi.org/10.1029/2020jb019770

Borzì, A. M., Minio, V., Cannavò, F., Cavallaro, A., D'Amico, S., Gauci, A., et al. (2022). Monitoring extreme meteo-marine events in the Mediterranean area using the microseism (Medicane Apollo case study). *Scientific Reports*, *12*(1), 21363. https://doi.org/10.1038/s41598-022-25395-9

Borzì, A. M., Minio, V., De Plaen, R., Lecocq, T., Alparone, S., Aronica, S., et al. (2024). Integration of microseism, wavemeter buoy, HF radar and hindcast data to analyze the Mediterranean cyclone Helios. *Ocean Science*, *20*(1), 1–20. https://doi.org/10.5194/os-20-1-2024

Borzì, A. M., Minio, V., De Plaen, R., Lecocq, T., Cannavò, F., Ciraolo, G., et al. (2024). Long-term analysis of microseism during extreme weather events: Medicanes and common storms in the Mediterranean Sea. *Science of the Total Environment*, *915*, 169989. https://doi.org/10.1016/j.scitotenv.2024.169989

Bromirski, P. D. (2001). Vibrations from the "perfect storm". *Geochemistry, Geophysics, Geosystems*, *2*(7). https://doi.org/10.1029/2000GC000119

Bromirski, P. D., Duennebier, F. K., & Stephen, R. A. (2005). Mid-ocean microseisms. *Geochemistry, Geophysics, Geosystems*, *6*(4). https://doi.org/10.1029/2004GC000768

Bromirski, P. D., Flick, R. E., & Graham, N. (1999). Ocean wave height determined from inland seismometer data: Implications for investigating wave climate changes in the NE Pacific. *Journal of Geophysical Research*, *104*(C9), 20753–20766. https://doi.org/10.1029/1999jc900156

Caloiero, T., & Aristodemo, F. (2021). Trend detection of wave parameters along the Italian Seas. *Water*, *13*(12), 1634. https://doi.org/10.3390/w13121634

Caloiero, T., Aristodemo, F., & Algieri Ferraro, D. (2019). Trend analysis of significant wave height and energy period in southern Italy. *Theoretical and Applied Climatology*, *138*(1–2), 917–930. https://doi.org/10.1007/s00704-019-02879-9

Caloiero, T., Aristodemo, F., & Ferraro, D. A. (2022). Annual and seasonal trend detection of significant wave height, energy period and wave power in the Mediterranean Sea. *Ocean Engineering*, *243*, 110322. https://doi.org/10.1016/j.oceaneng.2021.110322

Cannata, A., Cannavò, F., Moschella, S., Di Grazia, G., Nardone, G., Orasi, A., et al. (2020). Unravelling the relationship between microseisms and spatial distribution of sea wave height by statistical and machine learning approaches. *Remote Sensing*, *12*(5), 761. https://doi.org/10.3390/rs12050761

Cannata, A., Cannavò, F., Moschella, S., Gresta, S., & Spina, L. (2019). Exploring the link between microseism and sea ice in Antarctica by using machine learning. *Scientific Reports*, *9*(1), 13050. https://doi.org/10.1038/s41598-019-49586-z

Craig, D., Bean, C. J., Lokmer, I., & Möllhoff, M. (2016). Correlation of wavefield-separated ocean-generated microseisms with North Atlantic source regions. *Bulletin of the Seismological Society of America*, *106*(3), 1002–1010. https://doi.org/10.1785/0120150181

Cutroneo, L., Ferretti, G., Barani, S., Scafidi, D., De Leo, F., Besio, G., & Capello, M. (2021). Near real-time monitoring of significant sea wave height through microseism recordings: Analysis of an exceptional sea storm event. *Journal of Marine Science and Engineering*, *9*(3), 319. https://doi.org/10.3390/jmse9030319

De Leo, F., Briganti, R., & Besio, G. (2024). Trends in ocean waves climate within the Mediterranean Sea: A review. *Climate Dynamics*, *62*(2), 1555–1566. https://doi.org/10.1007/s00382-023-06984-4

Dorman, L. M., Schreiner, A. E., Bibee, L. D., & Hildebrand, J. A. (1993). Deep-water sea-floor array observations of seismo-acoustic noise in the eastern Pacific and comparisons with wind and swell. *In Natural physical sources of underwater sound: Sea surface sound*, 165–174. https://doi.org/10.1007/978-94-011-1626-8_14

Dumont, S., Le Mouël, J. L., Courtillot, V., Lopes, F., Sigmundsson, F., Coppola, D., et al. (2020). The dynamics of a long-lasting effusive eruption modulated by Earth tides. *Earth and Planetary Science Letters*, *536*, 116145. https://doi.org/10.1016/j.epsl.2020.116145

Epos-France, S. (1995). Epos-France broad-band network (RLBP). *Epos-France Seismological Data Centre*. [Dataset]. https://doi.org/10.15778/resif.fr

Ferretti, G., Barani, S., Scafidi, D., Capello, M., Cutroneo, L., Vagge, G., & Besio, G. (2018). Near real-time monitoring of significant sea wave height through microseism recordings: An application in the Ligurian Sea (Italy). *Ocean and Coastal Management*, *165*, 185–194. https://doi.org/10.1016/j.ocecoaman.2018.08.023

Ferretti, G., Zunino, A., Scafidi, D., Barani, S., & Spallarossa, D. (2013). On microseisms recorded near the Ligurian coast (Italy) and their relationship with sea wave height. *Geophysical Journal International*, *194*(1), 524–533. https://doi.org/10.1093/gji/ggt114

Gerstoft, P., Fehler, M. C., & Sabra, K. G. (2006). When katrina hit California. *Geophysical Research Letters*, *33*(17). https://doi.org/10.1029/2006GL027270

Golyandina, N., & Zhigljavsky, A. (2013). SSA for forecasting, interpolation, filtration and estimation. *SpringerBriefs in Statistics*, *71–119*, 71–119. Singular Spectrum Analysis for Time Series. https://doi.org/10.1007/978-3-642-34913-3_3

Grevemeyer, I., Herber, R., & Essen, H. H. (2000). Microseismological evidence for a changing wave climate in the northeast Atlantic Ocean. *Nature*, *408*(6810), 349–352. https://doi.org/10.1038/35042558

Gualtieri, L., Camargo, S. J., Pascale, S., Pons, F. M., & Ekström, G. (2018). The persistent signature of tropical cyclones in ambient seismic noise. *Earth and Planetary Science Letters*, *484*, 287–294. https://doi.org/10.1016/j.epsl.2017.12.026

Guerin, G., Rivet, D., van den Ende, M. P. A., Stutzmann, E., Sladen, A., & Ampuero, J. P. (2022). Quantifying microseismic noise generation from coastal reflection of gravity waves recorded by seafloor DAS. *Geophysical Journal International*, *231*(1), 394–407. https://doi.org/10.1093/gji/ggac200

Hasselmann, K. (1963). A statistical analysis of the generation of microseisms. *Reviews of Geophysics*, *1*(2), 177–210. https://doi.org/10.1029/RG001i002p00177

Haubrich, R. A., & McCamy, K. (1969). Microseisms: Coastal and pelagic sources. *Reviews of Geophysics*, *7*(3), 539–571. https://doi.org/10.1029/RG007i003p00539

Institut Cartogràfic i Geològic de Catalunya. (1984). Catalan seismic network. *International Federation of Digital Seismograph Networks*. [Dataset]. https://doi.org/10.7914/SN/CA

Instituto Português do Mar e da Atmosfera, I. P. (2006). Portuguese national seismic network. *International Federation of Digital Seismograph Networks*. [Dataset]. https://doi.org/10.7914/SN/PM

Istituto Nazionale di Geofisica e Vulcanologia (INGV). (2005). Rete sismica Nazionale (RSN). [Dataset]. https://doi.org/10.13127/SD/X0FXNH7QFY

Janiszewski, H. A., Eilon, Z., Russell, J. B., Brunsvik, B., Gaherty, J. B., Mosher, S. G., et al. (2023). Broad-band ocean bottom seismometer noise properties. *Geophysical Journal International*, *233*(1), 297–315. https://doi.org/10.1093/gji/ggac450

Korres, G., Ravdas, M., & Zacharioudaki, A. (2019). Mediterranean Sea waves hindcast (CMEMS MED-waves). *Copernicus Monitoring Environment Marine Service (CMEMS)*. [Dataset]. https://doi.org/10.25423/CMCC/MEDSEA_HINDCAST_WAV_006_012

Lepore, S., & Grad, M. (2018). Analysis of the primary and secondary microseisms in the wavefield of the ambient noise recorded in northern Poland. *Acta Geophysica*, *66*(5), 915–929. https://doi.org/10.1007/s11600-018-0194-2

Lin, J., Lin, J., & Xu, M. (2017). Microseisms generated by super typhoon Megi in the western Pacific Ocean. *Journal of Geophysical Research: Oceans*, *122*(12), 9518–9529. https://doi.org/10.1002/2017JC013310

Longuet-Higgins, M. S. (1950). A theory of the origin of microseisms. *Philosophical Transactions of the Royal Society of London - Series A: Mathematical and Physical Sciences*, *243*(857), 1–35. https://doi.org/10.1098/rsta.1950.0012

MedNet Project Partner Institutions. (1990). Mediterranean very broadband seismographic network (MedNet). Istituto Nazionale di Geofisica e Vulcanologia (INGV). [Dataset]. https://doi.org/10.13127/SD/FBBBTDTD6Q

Minio, V., Borzì, A. M., Saitta, S., Alparone, S., Cannata, A., Ciraolo, G., et al. (2023). Towards a monitoring system of the sea state based on microseism and machine learning. *Environmental Modelling and Software*, *167*, 105781. https://doi.org/10.1016/j.envsoft.2023.105781

Moschella, S., Cannata, A., Cannavò, F., Di Grazia, G., Nardone, G., Orasi, A., & Gresta, S. (2020). Insights into microseism sources by array and machine learning techniques: Ionian and Tyrrhenian Sea case of study. *Frontiers in Earth Science*, *8*, 114. https://doi.org/10.3389/feart.2020.00114

Munk, W. H. (1944). Proposed uniform procedure for observing waves and interpreting instrument records. *Scripps Institution of Oceanography, Wave Project Rep*, *26*, 22.

Oliver, J., & Page, R. (1963). Concurrent storms of long and ultralong period microseisms. *Bulletin of the Seismological Society of America*, *53*(1), 15–26. https://doi.org/10.1785/BSSA0530010015

Pratt, M. J., Wiens, D. A., Winberry, J. P., Anandakrishnan, S., & Euler, G. G. (2017). Implications of sea ice on Southern Ocean microseisms detected by a seismic array in West Antarctica. *Geophysical Journal International*, *209*(1), 492–507.

Reguero, B. G., Losada, I. J., & Méndez, F. J. (2019). A recent increase in global wave power as a consequence of oceanic warming. *Nature Communications*, *10*(1), 205. https://doi.org/10.1038/s41467-018-08066-0

Retailleau, L., Boué, P., Stehly, L., & Campillo, M. (2017). Locating microseism sources using spurious arrivals in intercontinental noise correlations. *Journal of Geophysical Research: Solid Earth*, *122*(10), 8107–8120. https://doi.org/10.1002/2017jb014593

Retailleau, L., & Gualtieri, L. (2019). Toward high-resolution period-dependent seismic monitoring of tropical cyclones. *Geophysical Research Letters*, *46*(3), 1329–1337. https://doi.org/10.1029/2018GL080785

Retailleau, L., & Gualtieri, L. (2021). Multi-phase seismic source imprint of tropical cyclones. *Nature Communications*, *12*(1), 2064. https://doi.org/10.1038/s41467-021-22231-y

Rusu, L. (2024). An analysis of the expected wave conditions in the mediterranean sea in the context of global warming. *Ocean Engineering*, *301*, 117487. https://doi.org/10.1016/j.oceaneng.2024.117487

Saprykina, Y., Shtremel, M., Aydoğan, B., & Ayat, B. (2019). Variability of the nearshore wave climate in the eastern part of the Black Sea. *Pure and Applied Geophysics*, *176*(8), 3757–3768. https://doi.org/10.1007/s00024-019-02143-1

Shabtian, H. S., Eilon, Z. C., & Tanimoto, T. (2023). Seasonality of California central coast microseism.

Stutzmann, E., Schimmel, M., Patau, G., & Maggi, A. (2009). Global climate imprint on seismic noise. *Geochemistry, Geophysics, Geosystems*, *10*(11). https://doi.org/10.1029/2009gc002619

Vaglio Laurin, G., Francini, S., Luti, T., Chirici, G., Pirotti, F., & Papale, D. (2021). Satellite open data to monitor forest damage caused by extreme climate-induced events: A case study of the vaia storm in northern Italy. *Forestry: International Journal of Financial Research*, *94*(3), 407–416. https://doi.org/10.1093/forestry/cpaa043

Vega, M. J., Alvarez-Silva, O., Restrepo, J. C., Ortiz, J. C., & Otero, L. J. (2020). Interannual variability of wave climate in the Caribbean Sea. *Ocean Dynamics*, *70*(7), 965–976. https://doi.org/10.1007/s10236-020-01377-1

Welch, P. (1967). The use of fast fourier transform for the estimation of power spectra: A method based on time averaging over short, modified periodograms. *IEEE Transactions on Audio and Electroacoustics*, *15*(2), 70–73. https://doi.org/10.1109/TAU.1967.1161901

Zhang, J., Gerstoft, P., & Bromirski, P. D. (2010). Pelagic and coastal sources of P-wave microseism: Generation under tropical cyclones. *Geophysical Research Letters*, *37*(15). https://doi.org/10.1029/2010GL044288